Macromolecular Theory and Simulations / Volume 21, Issue 5 / p. 285-301

Full Paper | Full Access

trans–cis and *trans–cis–trans* Microstructure Evolution of Azobenzene Liquid-Crystal Polymer Networks

Hongbo Wang,Kyung Min Lee,Timothy J. White,William S. Oates

First published: 21 December 2011
https://doi.org/10.1002/mats.201100089
Citations: 17

Abstract

The photomechanics of azobenzene LCNs is modeled using a nonlinear continuum mechanics approach that couples photoisomerization of liquid crystal domain structures with light absorption and deformation of a glassy polymer network. The effects during UV-stimulated *trans–cis* photomechanical deformation versus blue-green light (*trans–cis–trans*) photomechanical deformation are simulated. Different bending deformation is predicted by assuming liquid-crystal order/disorder behavior during *trans–cis* photoisomerization in comparison to light-polarization-driven reorientation of the *trans* phase during potential *trans-cis-trans* photoisomerization. Light-controlled deformation mechanisms offer support for improved control of photo-responsive morphing structures with a single blue-green polarized light source.

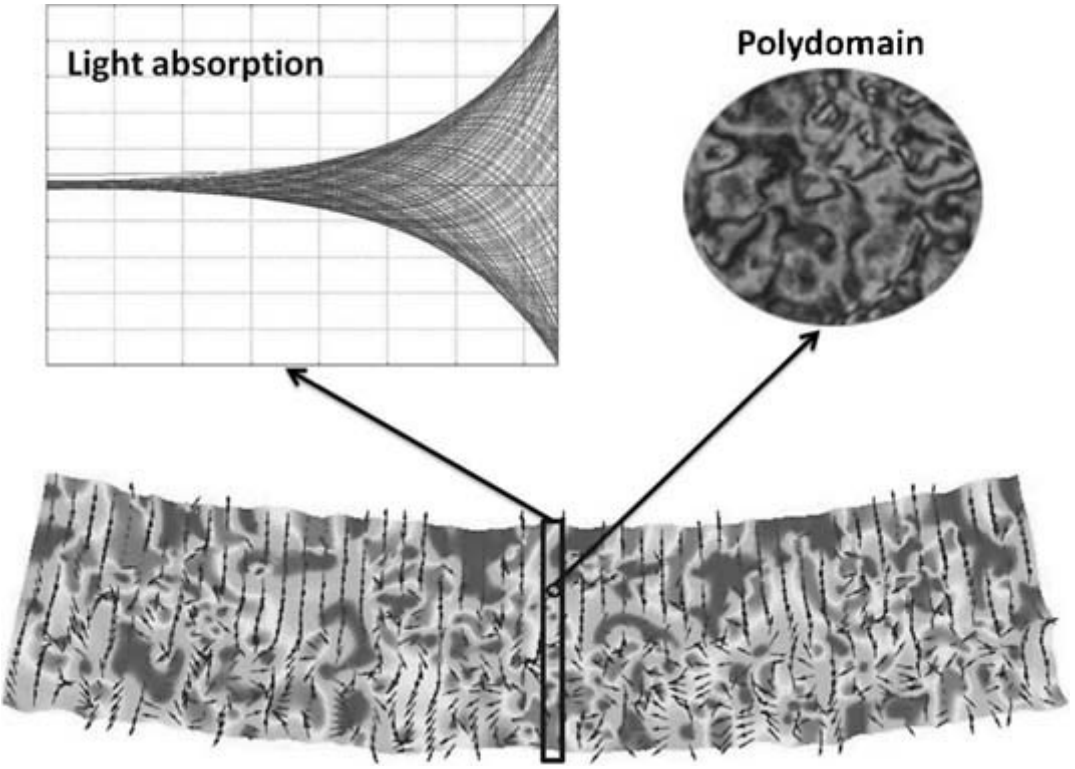

1. Introduction

Liquid crystal polymer networks (LCNs) exhibit a number of fascinating material characteristics for artificial muscle, sensing, and adaptive optics applications.[1], [2] These materials are classified by a large number of field-coupled mechanical characteristics including photomechanical coupling,[3]-[5] flexoelectricity,[6] thermal shape memory,[7] electrostriction,[8], [9] and chemically induced deformation.[10] Light induced deformation has received considerable attention recently due to its unique functionality for remote and spatial control of adaptive structures.[2], [3], [11]-[17] Photomechanical responses in liquid crystalline polymer networks have been observed by either doping a photochromic guest molecule into a LCN (guest/host) or by covalently bonding a photochromic mesogenic monomer into the network. Recent research efforts have primarily focused on liquid crystalline polymer networks in which a photochromic mesogenic monomer, azobenzene in all examples to date, is copolymerized into an elastomeric siloxane network or a glassy acrylate network. Within these glassy or elastomeric azobenzene-functionalized liquid crystal polymer networks, incident light energy is transduced into mechanical output by photoisomerization of azobenzene.

Photoisomerization (*trans–cis*) by UV light irradiation of azobenzene liquid crystals is known to strongly affect the order parameter of conventional liquid crystal (fluidic) systems, in certain cases causing photoinduced, isothermal phase transitions to the lower-ordered states.[18] These photoinduced, order-decreasing phase transitions to UV light exposure have been observed in elastomeric, azobenzene-functionalized liquid crystal polymer networks as evident in the work

described in ref.[19] Comparatively, the association of the order parameter and UV light exposure in glassy, azobenzene-functionalized liquid crystal polymer networks is not as well studied. It has been experimentally shown that the large amplitude photomechanical responses observed in these materials do not result in large changes to the order parameter of the system. The work presented here focuses on distinguished photomechanical responses observed in glassy, azobenzene-functionalized liquid crystal polymer networks that are exposed to a comparatively higher wavelength of light (442 nm). Light at this wavelength is known to induce both *trans–cis* and *cis–trans* isomerization of azobenzene, as these photons are absorbed nearly equivalently by *trans* and *cis* isomers for this class of azobenzene materials. When light of this wavelength is linearly polarized, reorientation of azobenzene normal to the electric field vector of the incident photons results in a statistical reorientation of azobenzene chromophores. This reorientation occurs due to repeated *trans–cis* and *cis–trans* isomerization cycles, which due to the dichroic absorption of both *trans* and *cis* azobenzene, result in a statistical buildup of azobenzene chromophores aligned normal to the incident polarization of the illuminating source. This phenomenon, often described as the Weigert effect, has been widely leveraged in fluids, elastomeric polymers, and glassy polymers–in applications ranging from liquid crystal alignment layers to surface relief gratings and photomechanical actuation.[20] Despite wide utility and a number of experimental examinations, the ability of azobenzene to reorient, especially in glassy and anisotropic media, remains surprising. As such, this work aims to quantify light induced deformation in azobenzene liquid crystal polymer networks using a microscale modeling approach. The model is motivated by polydomain azobenzene polymer network film experiments described in ref.[21] which illustrated symmetric bi-directional bending as the polarization of light with a 442 nm wavelength was rotated 90°. The symmetry associated with this bending strongly suggests a reorientational effect is responsible for the bi-directional bending; however, a careful assessment of the coupling between the polymer network, liquid crystal evolution during either *trans–cis* or *trans–cis–trans* photoisomerization, and polarization orientation of the light source is desired to elucidate differences in the observed photomechanical deformation.

Previous model development for photo-responsive polymers has ranged from continuum to molecular modeling with emphasis on quantifying the deformation based on the underlying liquid crystal re-orientation or photochemical effects. Toshchevikov et al.[22] presented a molecular dynamic approach to modeling photomechanical liquid crystal polymers. Viscoelasticity of the elastomer coupled with molecular features of the azobenzene molecules illustrated permanent deformation predictions as a function of temperature. Continuum modeling has also been conducted on the photochemical behavior[15] and liquid crystal network photomechanics.[14], [16], [23], [24] Most prior work has focused on the order-disorder behavior and manifestations most commonly described as photomechanically actuated bending cantilevers that are strongly dependent on the temporal rate and spatial attenuation of light within the

material. This behavior is often nonlinear due to dichroism (anisotropic light absorption) and does not typically follow the classic Beer-Lambert light attenuation model.[25, 26]

The model presented here is based on a microscale director force balance that is coupled to mechanics of the host polymer network; see ref.[27, 28] for details. The model is extended to include electro-magnetic light absorption to understand the differences in deformation during either *trans–cis* or *trans–cis–trans* photoisomerization. The liquid crystal molecular orientation is treated as an effective director as shown in Figure 1. This is a microscale homogenization of the molecular features of the material. A vector order parameter is used to approximate behavior typically described by a second order liquid crystal tensor, where Q is a scalar order parameter and n_i is the normalized liquid crystal director.[1, 29] More details on variational methods using this approach can be found in ref.[30, 31] This liquid crystal elastomer model (excluding photomechanics) has also been considered theoretically by defining Q as a tunable parameter to quantify compatible strain relations.[32] In this analysis, evolution of the effective director (referred to as the director for brevity) is modeled by neglecting independent evolution laws for both Q and n_i and instead introducing an effective microscale director that may vary in magnitude between zero and one. A traceless second order liquid crystal tensor is defined in an undeformed reference configuration while allowing for photomechanical model predictions during order-disorder processes. For further details on the distinctions between modeling Q and n_i as order parameters, see ref.[30] Another key distinction with the proposed model is the use of a compressible mechanical energy function for the host polymer network. Prior work has used a hyperelastic neo-Hookean incompressible model that is coupled to the liquid crystal domains.[28] Here, the model is modified to include an elastic mechanical energy to model a glassy photomechanical polymer network which may not necessarily follow incompressible material behavior. This is shown to be important during deformation imposed by *trans-cis* photoisomerization. For comparisons to other liquid crystal elastomer modeling frameworks; see ref.[1, 33, 34]

Figure 1

Illustration of the nonlinear continuum mechanics model and underlying liquid crystal elastomer network. Mechanical loading is shown by traction T_i. Light stimuli are shown by the Poynting vector I_i and electric field E_i. An internal mechanical body force is denoted by B_i. The order of the director and orientation depends on the wavelength and polarization of light.

Other relevant theoretical and experimental work on the absorption characteristics of azobenzene polymer networks are described in ref.[16], [25] These analyses include coupled evolution of liquid crystal *trans* and *cis* phases using a population dynamics equation that accommodates different transition rates for *trans–cis* and *cis–trans* transformations. In addition, a one-dimensional Poynting vector balance was used that assumes the divergence of the Poynting vector is predominantly due to light absorption of the azobenzene chromophores. In this analysis, certain electromagnetic Maxwell relations are introduced to incorporate polarized light effects, nonlinear light absorption, and time-averaged fields that affect the deformation of the azobenzene LCN film. Time-averaged electromagnetic fields are coupled with the liquid crystal director force balance and linear momentum of the polymer network to simulate a first order photoisomerization reaction rate and subsequent photomechanical deformation. A single time constant is introduced to model the photoisomerization of the azobenzene mesogens; see ref.[35], [36] for detailed analyses of these rate effects. Certain scaling relations are introduced to focus on the slower polymer deformation time scales by time-averaging the faster electromagnetic light waves with the slower varying polarized light field.

In the following sections, the photomechanical governing equations are summarized using linear momentum of the azobenzene liquid crystal network, a liquid crystal director force balance, and time-dependent electro-magnetics to provide a set of balance laws and field equations that incorporate photomechanical deformation, liquid crystal coupling, and polarized light interactions. This is followed by a description of the energy function and constitutive relations governing photostrictive liquid crystal behavior and light interaction within the liquid crystal network. Estimates on *trans–cis* and *trans–cis–trans* photomechanical deformation of a representative volume element are first described followed by a fully-coupled finite element phase field model of polydomain liquid crystal polymer network films exposed to polarized light. Discussion and Conclusion are given in the final two sections.

2. Governing Equations

The governing equations for the photomechanical LCN include the linear momentum balance, a liquid crystal microscale force balance, and time-dependent and time-averaged electro-magnetic field equations governing light absorption of the liquid crystal isomers. Whereas thermal effects can play an important role when the material is exposed to high laser power, the model developed here focuses on isothermal behavior. In many cases, this is a reasonable approximation based on bi-directional bending data on the azobenzene liquid crystal networks under consideration; see ref.[37], [38]

Whereas small to moderate strain will be of primary interests in the glassy liquid crystal network, nonlinear deformation is initially included within the modeling framework using the deformation gradient

((1))

where a material particle occupies the spatial point defined by at time t relative to the reference material point X_K.39 Finite deformation and rotational invariance is used to determine a set of coupling relations between deformation and the liquid crystal director. Later, limits to infinitesimal strain are taken to assess the effect of nonlinear geometric coupling on light induced deformation during different photoisomerization processes.
Conservation of linear momentum is defined in the reference domain as

((2))

where B_i is the body force and traction is denoted by T_i. The density is ρ_0 and velocity is v_i. The traction is applied over the boundary of the domain in the reference configuration which is denoted by Γ_0. Similarly, the volume in the reference configuration is denoted by Ω_0.

Traction is related to nominal stress in the reference configuration according to the relation, where is the unit normal pointing outwards on the material surface. This traction will be referred to by “mechanical” loads on the surface; however, the internal stress may include effects from the liquid crystals and polymer network.

By substitution of the traction relation and application of the divergence theorem to Equation 2, the linear momentum must satisfy

((3))

subject to traction or fixed displacement boundary conditions on Γ_0.
The mechanical relations are coupled with microscale liquid crystal domain structure re-orientation. A director force balance law is introduced to accommodate local changes in the azobenzene liquid crystal director. As illustrated in Figure 1, a liquid crystal director is introduced to model microscale liquid crystal structure embedded within the polymer network. In the reference configuration, the director force balance is

((4))

where the micro-stress tensor is and the extrinsic and intrinsic director body forces are denoted by and , respectively. All microstructure field quantities in the reference configuration are denoted with uppercase indices and . This will be distinguished from microstructure fields in the deformed configuration using lower case indices and no tilde. This balance relation is similar to an analysis given in ref.27 except that rotational inertial effects are neglected and an objective rate will be introduced on the director. In addition, the external body force is used to treat forces on the *trans* isomer induced by polarized light. This will be used to quantify polymer deformation during *trans–cis–trans* photoisomerization as discussed in Section 3.2. Rotational invariance must be introduced on the director for finite deformation problems. Rotational invariance is satisfied using 28 where is the director in the deformed configuration. The time derivative of this rotational invariant director requires objective rates as defined by

((5))

where H_{iK} is the inverse deformation gradient and . This objective rate includes the divergence of velocity for compressible deformation processes (i.e.,) and the velocity gradient that is defined by .39 A similar objective rate is often used in modeling field rates during finite deformation of electromagnetic solids.40

The relation described by Equation 5 is used in formulating the dissipative energy relation. This dissipative energy relation is implemented in Equation 4 within the term defined by as a function of the evolution rate of the vector order parameter . The dissipative energy is defined as where β_{IJ} is the inverse mobility tensor. It is assumed that this tensor is isotropic () to explore the salient features governing this problem. In general, dependence on the liquid crystal *trans* or *cis* phase may influence the inverse mobility constant.29, 41 By taking the variation of this dissipative energy function, a dissipative term within the microscale body force is obtained as described below.

The liquid crystal work conjugate relations to are defined by including a conservative force. In general, both conservative and dissipative forces are included in . These relations are given by

((6))

where the first term on the right hand side is a conservative force that will be later defined by a thermodynamic potential. The second term is a rate dependent dissipative force. The inverse mobility factor β_{IJ} must be positive definite based on the Clausius-Duhem inequality.28
By application of the divergence theorem on the left hand side of Equation 4, the director force balance in the reference volume is

((7))

where Equation 6 has been applied. The boundary conditions include on Γ_0. This assumes the force balance is applicable within the continuum limit of arbitrarily small representative volume elements of the homogenized director illustrated in Figure 1.
Electro-magnetic field relations are also introduced to model polarized light absorption within the material. The form of the electro-magnetic equation used to model light propagation neglects reflection of light on the material surface and therefore only considers the amount of light that is transmitted into the LCN. This can be modeled using Faraday's law of induction

((8))

where the electric field in the reference frame is , the current density is denoted by , and the polarization is denoted by . The permittivity of free space is denoted by and the magnetic permeability coefficient, μ, is assumed to be linear.
The azobenzene liquid crystal polymer network is typically non-conductive; therefore, the current density is defined to be zero. Normally, bound charges associated with polarization are modeled as weakly damped harmonic oscillators.42, 43 Here, we focus on absorption processes that occur over a small wavelength regime near the experimental ultra-violet and 442 nm wavelengths. This allows the field-polarization relation to be approximated by only the dissipative component within the weakly damped oscillator using

((9))

where the absorption tensor is denoted by α_{ij} and will be later defined to be a function of the liquid crystal director to accommodate dichroic (e.g., anisotropic) absorption. This tensor is used to predict the amount of light absorption within the liquid crystal polymer network. In general, this tensor will also be a function of the wavelength of light. We treat this difference phenomenologically, as described in the numerical section.
The relation given by Equation 8 is simplified by assuming zero free charge density, the permittivity is homogeneous, and . Under these assumptions, substitution of Equation 9 into Equation 8 gives

((10))

using the identity and . The approximation given by the last term on the right hand side assumes that the electric field varies at a much faster rate than changes in the absorption tensor during liquid crystal evolution. The boundary conditions for this equation consist of a tangential oscillating electric field on the material surface due to the light source.

In summary, Equation 3, 7, and 10 are implemented in the phase field finite element model to predict the nonlinear mechanics of the photomechanical liquid crystal polymer network. A significant difference in time scales exist between the electromagnetic light wave frequency (≈700 THz), liquid crystal photoisomerization (10 ps), and polymer deformation (ms to s). The interactions between the azobenzene chromophores and polymer network are of primary concern, thus a time-averaged polarized light field equation will be introduced and coupled with the electromagnetic equation to calculate the average decay of light through the material. This time-averaged light field is used in applying forces and phase transformations to the liquid crystals to quantify photomechanical deformation during *trans–cis* and *trans–cis–trans* photoisomerization. These relations are given in the following section. The free energy and energy dissipation relations used to predict photomechanical deformation are also discussed in the following section. These relations will be used to obtain theoretical estimates on photomechanical deformation that are then compared to detailed photomechanically coupled phase field numerical simulations.

3. Free Energy and Constitutive Relations

The free energy function used in the model is decomposed into terms that define energy associated with stretching the host polymer network and the azobenzene liquid crystal domain structures. The total free energy is written per reference volume as

((11))

where the mechanical energy from stretching the polymer is denoted by and the liquid crystal free energy is denoted by . The internal state variables include the deformation gradient F_{iK}, and liquid crystal coupling via and . The liquid crystal tensor is used to describe nematic phase liquid crystal behavior and is a gradient on the liquid crystal director that models polydomain defect energetics. The tilde denotes that these order parameter relations are defined in the reference configuration. Electric fields are not included in the free energy since only dissipative absorption effects are included in the electromagnetic Equation 10. Photochemical *trans–cis* phase transformations from polarized light will be introduced within the liquid crystal Landau-deGennes free energy while *trans–cis–trans* effects due to polarized light will be modeled using the extrinsic body force () within the liquid crystal director force balance given in Equation 4. The liquid crystal second order tensor is defined in the reference domain by

((12))

where δ_{IJ} is the Kronecker delta. The constant n_0 is the equilibrium director value that is defined in an undeformed reference state. It depends on the liquid crystal free energy parameters that are explicitly defined in the following section. This tensor is traceless in an undeformed reference state for any equilibrium director value –1; however, nonzero deformation does not guarantee exact traceless properties in a currently deformed configuration. More comments on this approximation are given in Section 5.

3.1. Liquid Crystal Polymer Network Energy

A Landau-deGennes energy function is introduced within Equation 11 to determine the liquid crystal director orientation and coupling to the polymer network. Only isothermal processes are considered. In the reference configuration, the free energy function is

((13))

where , and $c_{IJKLMNRS}$ are phenomenological tensors that depend on the deformation gradient such that objectivity of the free energy function is satisfied. An additional dependence has been

introduced using a time-averaged electric field and the director . The time-averaged field equation is determined directly from the electric field given in Equation 10 which is discussed in subsequent paragraphs. This functional dependence is introduced to induce reductions in the microscale director order during *trans–cis* photoisomerization.
The higher-order tensors in Equation 13 are difficult to determine experimentally, therefore, a reduced set of coefficients are determined from a free energy expression in the spatial configuration. Using a rotational invariant liquid crystal tensor relation, , the free energy in the spatial domain is

((14))

per current volume where the dependence on and in *a* and *b* has been omitted for brevity. Using the identity, ,44 the correlation between the phenomenological constants is

((15))

where the Green deformation tensor, , has been introduced.39 Whereas these tensors range from fourth to eighth order, only three phenomenological constants are implemented in the numerical model.
Reduction in order of the microscale director within each liquid crystal domain (i.e., regions of like director orientation) are defined to depend on the polarization orientation of the time averaged electric field. The functional form of the time-averaged electric field coupling with the Landau-deGennes constants is

((16))

such that reductions in nematic order only occur when the time-averaged, electric field is parallel to the director. Note that the quadratic and linear dependence of and within *a* and *b* is implemented to restrict liquid crystal deformation to always be prolate during order-disorder processes. More detailed discussions for this restriction are given in the paragraph following Equation 23.

The time-averaged electric field introduced in Equation 13 is determined from a first-order reaction rate equation

((17))

where τ^{ph} is a time constant that is set to a value that is slower than the electromagnetic wave speed and comparable to the time constant of the liquid crystal domain structure mobility. This value is chosen to ensure a constant, time-averaged field during constant light exposure as will be illustrated numerically in Section 4.2.1.

A relation describing the liquid crystal coupling to the host elastomer is obtained from the definition of the nominal stress, .44 For brevity, the liquid crystal nominal stress based on Equation 13 is converted to a liquid crystal Cauchy stress relation using .39 The liquid crystal Cauchy stress is

((18))

Some comments are in order to illustrate how this liquid crystal stress gives anisotropic deformation as a function of the true liquid crystal tensor defined by . The true equilibrium director is approximated in the spatial domain using the work conjugate relation which is equal to zero at equilibrium. The equilibrium director value is then

((19))

where only the positive root within the parenthesis is considered. The form implemented here leads to anisotropic liquid crystal stress when this relation is substituted into Equation 18. Also note that as the equilibrium director goes to zero, . This assumes a reference isotropic phase as the *cis* phase where n_0 is defined to be zero. This stress coupling leads to positive deformation along the director orientation and contraction orthogonal to the director under certain restrictions governed by the free energy parameters as described after introducing the polymer elastic energy.

The equilibrium deformed shape of the liquid crystal network requires balancing the liquid crystal stress with mechanical stresses due to the polymer network. The mechanical energy of

the polymer network is assumed to be compressible and linear elastic since the polymer is glassy. For the small strain limit, the elastic free energy of the glassy polymer network is

((20))

where E and v are the elastic modulus and Poisson ratio. Infinitesimal strain is denoted by ε_{ij}. Small strain, ε_{ij}, is considered for the glassy polymer since these materials typically exhibit 1% strain or less in the glassy state. However, the theory can be extended to finite deformation by changing the elastic energy function. This approximation does not influence the coupling based on the Landau energy function. The mechanical Cauchy stress relation is given by the relation

((21))

Based on this stress relation, the nominal and Cauchy mechanical stresses (and , respectively) are determined and implemented in the balance equations using standard nonlinear continuum relations.[39], [44] Note that the total Cauchy stress is denoted by where a similar relation exists for the nominal stresses.

It is shown by balancing the mechanical and liquid crystal Cauchy stresses, that anisotropic deformation is predicted by the model. Consider a uniformly aligned azobenzene liquid crystal polymer network (i.e., monodomain) in the X_3 direction. This gives and . In the case of equilibrium deformation under zero applied traction, the total Cauchy stress is zero (). By solving for the spontaneous strain from the director coupling,

((22))

and for illustrative purposes, the spontaneous strain reduces to the following relation in the limit of incompressiblity (i.e., $v = 0.5$)

((23))

therefore must be satisfied to obtain prolate liquid crystal network deformation in the limit of incompressibility. A similar but more complex relation exists for compressible materials based on Equation 22. Figure 2(a) schematically illustrates the concept of deformation induced during *trans–cis* photoisomerization for a set of Landau-deGennes parameters.

Figure 2

(a) Idealized concept of deformation from a *trans* to *cis* phase and the corresponding polymer deformation of a representative volume element. (b) Change of the director equilibrium value over the range of normalized light intensities I. A set of parameters were chosen such that $n_0 = 1$ at $I = 0$.

Since we consider polydomain films, interactions near twinned domain structures are modeled by including the single constant Frank elastic energy function. This is implemented in the computational model using a scalar gradient penalty on the first order gradient of the director

((24))

where K is the Frank elastic constant that equally defines penalties on splay, twist, and bend of the liquid crystal director.1, 29 We have neglected any coupling between deformation and the Frank elastic constant since this coupling is normally smaller than the liquid crystal stress in Equation 18.

3.2. *trans-cis-trans* Microstructure Coupling

The previous section described a Landau-deGennes free energy that was coupled to polarized light and deformation to model *trans–cis* photomechanical deformation. As the light intensity increases toward unity, the non-zero free energy minimum wells are reduced to a single well at $n_0 = 0$ as defined in Equation 19 and illustrated in Figure 2(b). This model is primarily relevant to the ultraviolet wavelength.

An additional effect of polarized light induced forces is introduced here using the external body force previously defined within Equation 4. This behavior is assumed to occur when the wavelength of light overlaps the *cis* and *trans* absorption bands creating interactions between the two phases during polarized light exposure. Typically, the photoisomerization process is considered as a statistical process that occurs over time scales between the light frequency and

phase transformation process. These time scales are much shorter than the polymer deformation rates and are therefore treated in a time-average sense using the time-average field . The driving force for *trans* reorientation is motivated by dipole forces that occur as *cis* phase isomers interact with the polarized light; see ref.20 for a similar dipole force model. During *trans–cis* photoisomerization, it is assumed that an electric dipole is induced orthogonal to the *trans* phase director in the direction of the kinked *cis* phase. The average dipole force, in terms of the polarization, is defined by

((25))

where the polarization describes the nominal *cis* dipole averaged over a representative volume element. Assuming the rotational field effect from time dependent magnetic induction is negligible relative to the dipole contribution to the force, the second term on the right hand side of the equation can be neglected. This leads to dipole energy: such that the energy is reduced as the dipole aligns with the time-averaged polarized field. For the case of *trans–cis–trans* photoisomerization, the schematic in Figure 3 illustrates the propose reorientation behavior. Once a *cis* dipole is induced during an intermediate *trans-cis* photoisomerization, the dipole force induces alignment as shown during steps 2–3 in Figure 3. During subsequent *cis–trans* photoisomerization (in a statistical sense), the *trans* phase director is orientated in a plane that is orthogonal to the direction of polarized light, as seen in step 4 in Figure 3.

Figure 3

Open in figure viewer | PowerPoint

Schematic of the proposed *trans–cis–trans* driving force induced by a *cis* dipole under the polarized light field . An electric dipole is assumed to be present during the intermediate *cis* phase [steps (2) and (3)]. The external polarized light field tends to rotate the dipole to align with the field in step (3). *cis–trans* relaxation is assumed to occur in step (4) for wavelengths that overlap the *cis* and *trans* absorption spectra (e.g., 442 nm).

In the present model, the polarization of the *cis* phase isomers is not explicitly modeled. A reduced-order approach is implemented where the dipole force is defined to be the external body force given in Equation 7 which penalizes a liquid crystal director aligned with the time-averaged field. This body force is phenomenologically equivalent to the dipole force and is defined by

((26))

where e_0 is a positive phenomenological parameter. This parameter is scaled such that the intrinsic body force in Equation 7 is of the same magnitude as .

4. Numerical Implementation

The governing equations are implemented numerically using two approaches. First, a representative volume element is analyzed under ideal azobenzene liquid crystal evolution to illustrate differences in homogeneous deformation during *trans–cis* and idealized *trans–cis–trans* reorientation. Second, nonlinear model predictions of polydomain structure evolution are given using a finite element phase field approach to predict photomechanical coupled deformation due to gradients in light attenuation through the thickness of a film. The effect of anisotropic absorption and rotation of the light polarization are quantified and compared with experimental observations when assuming a *trans–cis* or *trans–cis–trans* photoisomerization.

4.1. Representative Volume Element

A simplified LCN model that excludes explicit light coupling is presented first to quantify changes in deformation when assuming a *trans–cis* or *trans–cis–trans* photoisomerization process in a monodomain representative volume element. It is shown that *trans–cis* photoisomerization is unlikely to induce *symmetric* bi-directional bending; however, an idealized *trans–cis–trans* reorientation will induce bi-directional bending during uniaxial director reorientation (i.e., only reorientation in the plane of the film). This is in contrast to bi-axial reorientation defined as director evolution to a plane orthogonal to the polarization. It is important to note that the effective dipole force given by Equation 26 will promote bi-axial rotation. Dichroic absorption behavior is also neglected in this representative volume element model. A comparison of these simplifying assumptions will be compared to the fully coupled finite element phase field model presented in Section 4.2.

The results are computed for a fully ordered monodomain with $n_0 = 1$ over a representative volume element that is exposed to uniform light intensity. Similar results are obtained for a homogenized, microscale director that is less than one (i.e., $n_0 < 1$). Spontaneous strain is obtained by setting the total Cauchy stress to zero and solving for the spontaneous strain as a function of the liquid crystal director, Landau-deGennes free energy parameters, and light intensity. This requires numerically solving Equation 18, 19, and 22 as a function of changes in the director. For *trans–cis* photoisomerization, reductions in n_0 are computed by increasing the

intensity of light. For the case of idealized *trans* rotation, the director is assumed to rotate from the X_1 direction to the X_2 direction with no change in magnitude.

As illustrated in Figure 4, different photomechanical strains are predicted for *trans–cis* and *trans–cis–trans* photoisomerization. In Figure 4(a), the strain computed during rotation of the *trans* phase leads to symmetric positive and negative strain components. In contrast, *trans–cis* photoisomerization leads to a reduction in the order of the director and non-symmetric deformation parallel and orthogonal to the director orientation. This is expected since it is strongly dependent on the Poisson ratio of the polymer network. For example, in the limit of $v = 0.5$, the model predicts that the spontaneous strain magnitude (ε_0) initially parallel to the director shrinks by an amount $-\varepsilon_0$ while strain orthogonal to the director expands in both directions by the amount $\varepsilon_0/2$. Comparisons of these two photoisomerization processes suggest that the idealized *trans–cis–trans* uniaxial rotation would lead to bi-directional bending as the polarization of light is rotated from 0 to 90°. In contrast, *un*-symmetric bi-directional bending is expected to occur during *trans–cis* photoisomerization. More bending is expected to occur toward the light source due to the Poisson effect illustrated in Figure 4(b). This analysis is compared to the fully coupled photomechanical phase field model in the following section.

Figure 4

Open in figure viewer | PowerPoint

A comparison of spontaneous strain induced by changes in the liquid crystal director. In (a), the director is rotated 90° in the (X_1, X_2) plane from a reference state of a fully ordered monodomain originally aligned in the X_2 direction. In (b), the magnitude of the director is reduced to zero from a fully ordered reference state that is aligned with X_2.

4.2. Fully Coupled Phase Field Simulations

Prior to illustrating numerical results, the key governing equations are first summarized in the weak form for finite element phase field implementation. The liquid crystal polymer mechanics equations include

((27))

where weight functions w_i and g_I represent test functions for the displacement of the polymer network and the liquid crystal director, respectively. The first equation is linear momentum

where acceleration and body forces have been neglected. Mechanical surface traction is denoted by T_i. Note that s_{iK} denotes the total stress which includes elastic behavior and liquid crystal stress. The second equation is the liquid crystal director force balance. The boundary conditions for "micro" traction in Equation 27 are set to zero on all material surfaces.
The light absorption equation based on Equation 10 is also given in the weak form. This equation is coupled to the time-averaged field that is used in calculating the *trans–cis* or *trans–cis–trans* photoisomerization behavior. These two equations are

((28))

where the weight function for the time-dependent and time-averaged fields are h_I and m_I, respectively. The second equation defines the time-averaged polarized field. The light propagation equations include coupling to the liquid crystals through the absorption tensor . This tensor is defined by

((29))

where is the absorption constant perpendicular to the director and is the absorption constant parallel to the director. In the dichroic absorption simulation, we implement (nominally consistent with experimental values for azobenzene), but also compare this to the case of a finite with as an extreme limit. It will be shown that this dichroic model has a negligible effect on variations in light attenuation for the polydomain liquid crystal polymer network.
A quasi-three dimensional model is numerically implemented to predict photomechanical liquid crystal network behavior under polarized light stimuli. This includes plane stress mechanics and two dimensional light absorption while the liquid crystal director is modeled in three dimensions to predict bi-axial director evolution by including all three director components on a two dimensional geometry. Since the geometry is 2D, out-of-plane director gradients (i.e., and out-of-plane shear coupling are neglected. This provides an approximate method to quantify *trans–cis–trans* photoisomerization and bi-directional bending that is more computationally efficient than a fully-coupled, three dimensional model.

Table 1. Parameters used in the finite element model. The liquid crystal parameters include K as the distortional energy constant, a_0, b_0, and c as the Landau parameters, E and v as the

elastic modulus and Poisson ratio, respectively. The absorption coefficients are denoted by , , respectively.

Name	Value	Unit
K	5×10^{-8}	N
a_0	3.85×10^{7}	$N \cdot m^{-2}$
b_0	-2.8×10^{8}	$N \cdot m^{-2}$
c	4.08×10^{8}	$N \cdot m^{-2}$
E	1.35	GPa
v	0.35	
	2.4×10^{10}	$A \cdot C \cdot (Nm)^{-2}$
	6×10^{9}	$A \cdot C \cdot (Nm)^{-2}$

The parameters used in the model are given in Table 2. In the following sections, the light absorption characteristics are first modeled to describe differences in isotropic versus dichroic absorption. This behavior is then coupled to the liquid crystal phase field simulations and polymer mechanics. All photomechanical phase field simulations were conducted on a polydomain model for comparison with polydomain experiments. The geometry in all simulations is $75 \times 15\ \mu m^2$ which includes a typical film thickness and a subsection along the length of the film. The boundary conditions for the problem are illustrated in Figure 5. These boundary conditions allow for free bending using a roller boundary condition while applying light via the tangential field on the top surface. All simulations begin from an equilibrium polydomain configuration. The equilibrium polydomain state is obtained by running the model from initial random conditions with a director magnitude of . The initial conditions and polydomain equilibrium results are illustrated in Figure 6.

Table 2. A summary of the nominal bending angles computed using the phase field model during *trans-cis* and *trans-cis-trans* photoisomerization. and indicate that the polarization of the light is orthogonal and parallel to the long axis of the film, respectively. A positive sign of an angle indicates that the bending is away from the light.

Type	[°]	[°]

Type	[°]	[°]
trans–cis	9	−22
trans–cis–trans	30	−30

Figure 5

Open in figure viewer | PowerPoint

Schematic of the liquid crystal polymer network configuration used in the polydomain model. The cross-section view shows the finite element boundary conditions of a sub-set of the entire film. Simply supported mechanical constraints are applied to predict free displacement bending. The simulations include rotating the polarization of light in the X_1–X_3 plane.

Figure 6

Open in figure viewer | PowerPoint

Evolution of polydomain liquid crystal networks from an initial random distribution in (a) to the equilibrium state in (b). The surface plot corresponds to the director component . More detailed, colored version is in the Supporting Information.

4.2.1. Light Absorption and Time-Averaged Fields

The time dependent and time-averaged polarized light field equations in Equation 28 are first simulated for a *fixed* liquid-crystal polydomain domain structure based on Figure 6(b) results. The polydomain structure is held fixed during these simulations to analyze differences in light absorption when assuming isotropic or dichroic absorption. Absorption constants as a function of the director in Equation 29 are based on data for monodomains for polarized light at 442 nm.37

As previously noted, the large differences in time scales associated with the light wavelength and photomechanical response requires scaling the light frequency and absorption constants to simulate photomechanical deformation. This scaling was done to achieve the same field decay through the thickness at a time constant τ^{ph} that was slightly smaller than the dynamic response of the liquid crystal director. The scaled polarized light wave frequency was reduced

to a frequency (1.5 MHz) that was slightly larger than mobility associated with the time constant: s such that a time-averaged field is obtained from the polarized light waves which absorb into the polymer film. Note that this light frequency was arbitrarily chosen to facilitate numerical implementation.

In Figure 7, a comparison of the electro-magnetic light absorption through the material thickness is compared with the time-averaged field for the isotropic and dichroic absorption models. As shown in Figure 7(a), the time dependent electromagnetic wave for the anisotropic absorption model () is reduced in magnitude as the light propagates into the material from the right to the left. The lines in the plot represent a projection of waves along the entire length of the film. The first order time response of the time-averaged field is shown in Figure 7(b) for the isotropic and anisotropic models. A smooth first order increase in the time-averaged field is computed based on the scale polarized light field frequency and τ^{ph}.

Figure 7

Open in figure viewer | PowerPoint

(a) Example of the time-dependent field for the anisotropic absorption model. The electric field waves along the length of the film have been projected onto a two-dimensional plot to illustrate absorption through the 15 μm thickness. (b) The first order transient time response of the time averaged polarized field based on the polarized light waves.

In Figure 8, the spatial variation along the polydomain model illustrated in Figure 6(b) is shown to quantify variations in light intensity for the isotropic and dichroic models. For the absorption material parameters under consideration, Figure 8 shows that dichroic absorption is slightly weaker than isotropic absorption. In the extreme case of further penetration depths are predicted, but minimal changes relative to the dichroic and isotropic cases are predicted. It is noted that although the light model is fully coupled with the liquid crystal model through the absorption tensor, the relatively small differences in isotropic versus dichroic absorption is believed to be due to the polydomain structure.

Figure 8

Open in figure viewer | PowerPoint

The decay of the time-averaged light intensity along the thickness of the film for both the isotropic and anisotropic absorption models.

Due to the small differences in light attenuation for the different absorption tensors, isotropic absorption is coupled to the liquid crystal evolution and polymer mechanics model to simplify numerical simulations of photomechanics bending for both *trans–cis* and *trans–cis–trans* photoisomerization. This provides a qualitative estimate on light induced bending deformation. Additional discussion on this approximation is given after presenting the photomechanical bending results.

4.3. Fully Coupled Photomechanical Deformation

Photomechanical deformation is simulated using the phase field approach to quantify differences that occur during *trans–cis* and *trans–cis–trans* photoisomerization in a polydomain film. The models are simulated under free displacement boundary conditions with light applied on the top as illustrated in Figure 5. To facilitate computational efficiency, the small strain approximation is used to study the glassy polymer network. This is a reasonable assumption since photomechanical strain is typically on the order of 1% in these glassy films. This assumption allows the Landau coefficients in Equation 13 and 15 to be independent of the deformation gradient. This gives only one-way coupling where the liquid crystal Cauchy stress given by Equation 18 is still present, but any changes in the liquid crystal structure that may occur during large deformation is neglected. This is a reasonable approximation since no external mechanical loading is applied and deformation is only induced by internal liquid crystal director changes induced by light.

4.3.1. *trans–cis* Bending

In the following simulations, the effect of reductions in director order that are expected to occur during *trans–cis* photoisomerization are simulated to quantify bending under polarized light. The equilibrium director order is first plotted with no light present for comparisons to order reduction and light-induced bending during *trans–cis* photoisomerization. Figure 9 illustrates that the magnitude of the director is approximately uniform over the entire film prior to light exposure and has a local director value of . When the film is exposed to the light, the liquid crystal domains on the top side of the beam absorb light and change to a disorder *cis* state which is predicted as a reduction in the local director magnitude.

Figure 9

Open in figure viewer | PowerPoint

Distribution and magnitude of the liquid crystal director of the polydomain film prior to exposure to UV light. The surface plot is the magnitude of the director, . More detailed, colored version is in the Supporting Information.

Figure 10 illustrates differences in bending deformation as the direction of polarized light is rotated from the horizontal direction to the direction normal to the page. In Figure 10(a), relatively larger bending toward the light is observed due to the polarized light orientation . In this case, the light polarization is oriented in the horizontal direction which induces disorder of the domains aligned in the horizontal direction. This leads to contraction along the length of the film and bending toward the light. In comparison, when the polarized light source is aligned out-of-the page () reductions in the director component drives the film to bend away from the light source. The order reduction of leads to contraction out-of-the page and a relatively smaller expansion in the X_1 direction. Therefore, the amount of bending away from the light is smaller than the case where the beam bends toward the light.

Figure 10

Open in figure viewer | PowerPoint

A polydomain LCN beam exposed to polarized light during *trans–cis* photoisomerization. The surface plot is the director component and the final deformed state is shown based on initial conditions illustrated in Figure 6(b). (a) Bending toward the light source when (horizontal orientation), and (b) smaller bending away from the light source when (out-of-plane orientation). More detailed, colored version is in the Supporting Information.

The average bending angles for these two cases are compared in Table 2. In this table, the bending toward the light is −22°. This is attributed to the difference in contraction and expansion illustrated in Figure 2(a) and 4(b). The reduction of the liquid crystal order along and subsequent smaller expansion along the length of the film leads to a bending angle of 9° away from the light source. This table also summarizes two bending angles when assuming *trans–cis–trans* photoisomerization. It will be shown in the following section that the same set of material parameters leads to symmetric bending based on the phase field modeling framework.

4.3.2. *trans–cis–trans* Bending

If the UV light source is replaced by a blue laser light (e.g., 442 nm), symmetric forward and backward bi-directional bending has been observed experimentally as the polarization of light is rotated 90°.[21] Since this wavelength of light lies in the overlapping region of *trans–cis* and *cis–trans* isomerization processes, *trans–cis–trans* is expected to occur. Despite the lack of quantitative measurements of this process,[37] the phase field model is used to indirectly provide insight on deformation expected to occur during *trans–cis–trans* photoisomerization.

To simulate the photomechanical deformation during this photoisomerization process, the extrinsic body force discussed in Section 3.2 is introduced. Figure 11 illustrates

photomechanical free bending predictions when assuming *trans–cis–trans* photoisomerization. Figure 11(a) illustrates the initial polydomain structure prior to exposure to polarized light. In Figure 11(b), the polarized light is applied on the top surface in the out-of-page direction which induces liquid crystal domain structure reorientation onto the plane. This is expected since the extrinsic body force only penalizes domains aligned with the polarization of light (i.e.,) thus promoting *trans* phase reorientation to any orientation on the plane. The liquid crystal domains that rotate along the long axis of the film induce positive deformation and bending away from the light source as illustrated in Figure 11(b). If considering a size of the film that is similar to experimental results ($6 \times 1 \times 0.015$ mm^3 21), the bending angle is 30° assuming a constant curvature along the film length. Comparable results have been observed experimentally, when the polarization was orthogonal to the long axis of the film.

Figure 11

Open in figure viewer | PowerPoint

Bending of a polydomain LCN beam during *trans–cis–trans* photoisomerization due to rotating the polarization of blue-green light. The surface plot is the director component . (a) Initial state of the polydomain structure, (b) the polarized light points out-of-the-page, (c) the polarized light along the long axis of the beam, (d) the polarized light rotates back to the out-of-page direction. More detailed, colored version is in the Supporting Information.

The additional simulation results given in Figure 11(c,d) illustrate symmetric bi-directional bending when the polarization of light is rotated 90°. In Figure 11(c), the polarized light has been rotated to the X_1 (horizontal) direction and then rotated back to the out-of-page direction in (d). Figure 11(c), the liquid crystal domains stimulated by the polarized light parallel to the long axis of the beam rotate to either the out-of-page direction or the vertical direction. In contrast to the idealized representative volume element model in Section 4.1 where uni-axial reorientation was assumed, bi-axial reorientation of the *trans* phase isomers is predicted by the phase field model. This photoisomerization induces negative strain along the long axis regardless of reorientation from to or to and consequently bending toward the light. In Figure 11(d), the polarization of light is rotated back to the X_3 direction where the out-of-page liquid crystals are driven back toward the (,) directions again and the bending away from the light is repeated. However note in this case that only liquid crystals that reorient from to induce bending away from the light. The volume fraction of liquid crystals that evolved from to do not contribute to bending. The domains along only contribute to bending along this axis since the deformation is due to prolate interactions.

Since the increase of volume fraction of the liquid crystals in Figure 11(b) is less than the decrease of in Figure 11(c), asymmetric bi-directional bending is predicted by the model during the first few rotations of the polarization of light as shown Figure 12(a). The error bars on this plot represent the maximum and minimum calculated bending angles due to the irregular surface of the simulation that is due to the polydomain liquid crystals. Larger bending toward the light (negative angles) is predicted during the first few cycles since changes in both and contribute to this bending. In comparison, bending away from the light is only due to changes of the and director components as also illustrated in Figure 12(a). The increase in during this process limits the amount of positive bending. The macroscopic bending asymmetry is similar to predictions during *trans-cis* photoisomerization; however, upon multiple cycles of polarization rotation, the increase in volume fraction of per rotation is significantly reduced while the magnitude of change in and per cycle is approximately constant, see Figure 12(b). This change in director evolution leads to symmetric bi-directional bending.

Figure 12

(a) Bending angles at different time steps during polarization rotation of light based on the *trans–cis–trans* simulations. Note that the bending angles away from light are positive and bending toward the light is negative. (b) The corresponding time dependent evolution of the average magnitude of each component of the liquid crystal domains when *trans–cis–trans* isomerization occurs. Note that at 0.02, 0.06, 0.10, 0.14, 0.18, and 0.22 s polarized light is out-of-the-page. At 0.04, 0.08, 0.12, 0.16, and 0.20 s, the light is in the horizontal direction X_1.

5. Discussion

A computational analysis describing the differences in photomechanical deformation during *trans–cis* and *trans–cis–trans* photoisomerization has been modeled using a phase field approach that couples polymer deformation, polydomain liquid crystal domain structure evolution, and light absorption. The results illustrate subtle differences in bending deformation that are expected to occur as the wavelength of light changes from UV to blue-green. These differences are complicated by non-equilibrium liquid crystal evolution, polarized light driving forces, and elastic coupling between the glassy polymer network and liquid crystal domain structures. Qualitative bi-directional bending predictions were computed assuming *trans–cis* or *trans–cis–trans* photoisomerization during 90° polarization rotation of light. Similar to experiments,[21] symmetric bi-directional bending about the neutral (zero light) state was predicted during *trans–cis–trans* photoisomerization upon multiple rotations of the light polarization orientation. In contrast, asymmetric bi-directional bending was predicted when

assuming *trans–cis* photoisomerization where larger bending toward the light occurred. The *trans–cis* bending results were only achieved for a random *trans* phase polydomain state as the initial conditions. *Trans–cis* bending toward and away from the light during 90° polarization *rotation* could not be predicted with the model. This is because the order-disorder effect only occurs in liquid crystal domains aligned with the polarization. As the polarization of UV light is rotated 90°, an equal volume fraction of disorder occurs in all liquid crystal domains in the plane of the film exposed to light which severely limits bi-directional bending control.

The computational results were based on quasi-3D simulations that included 3D liquid crystal structure evolution on a 2D geometric domain under plane stress mechanics conditions. Plane stress conditions were chosen since most free bending experiments consists of light applied uniformly across the surface of the film and therefore do not exhibit a plane strain constraint. It is emphasized that the results are qualitative since large reorientation of liquid crystal domains was simulated. In glassy polymer networks, the change in the director may be much smaller; however, similar trends in deformation are expected under smaller volume fractions of liquid crystal evolution by scaling the Landau-deGennes free energy parameters to predict the correct amount of deformation. More quantitative fits are under investigation using solid state nuclear magnetic resonance measurements to further explore these material parameter uncertainties.

Based on the plane stress model that was coupled to the 3D liquid crystal domain structure evolution, the director reorientation during *trans–cis–trans* photoisomerization transitioned from asymmetric bi-directional bending to symmetric bending after repeated rotations of the light polarization. This occurred once the director component in the film thickness direction reached a quasi steady-state. The extrinsic liquid crystal body force only penalized the director to reorient to a plane that was orthogonal to the light polarization. This suggests a lower liquid crystal energy state would occur if all director components eventually aligned in the thickness direction upon multiple 90° polarization rotations. This competes however with the gradient of light through the thickness that will lead to increases in elastic energy due to director splay and bend and subsequent stress gradients through the film thickness. These gradients are typically larger than a linear strain gradient induced by pure bending since light absorption is a psuedo-exponential decay (exponential in the isotropic Beer-Lambert case). This latter mechanism was confirmed numerically as domains that reoriented to the X_2 (thickness direction) on the surface would propagate through the entire thickness while other domains would continue to reorient between and during light polarization rotation. The elastic mechanical energy was also calculated during the *trans–cis–trans* simulations and found to be initially large and decayed to a lower energy state as the bending angles became symmetric in correspondence with Figure 12. In terms of light absorption for UV and blue-green light, it is also important to note that differences in the absorption coefficients were neglected which are expected to influence quantitative predictions of photomechanical bending.

Other important energetic differences in reorientation between versus reorientation are the differences in the Frank elastic energy. In this analysis, the phase field simulations assumed a single Frank constant; however, different penalties for twist, splay, and bend have been measured for other nematic phase liquid crystals. It is noted that the penalty for twist is approximate 1.5 times lower that splay and bend for certain nematic liquid crystals.[29] This would promote reorientation and symmetric bi-directional bending during *trans* phase reorientation from blue-green light. Additional simulations were conducted using the three constant Frank elastic energy formulation and no significant difference in domain structure evolution was calculated. This is most likely because the Frank elastic driving force within is significantly smaller than the intrinsic body force in the director force balance. Moreover, pure twist is most likely complicated by simultaneous *trans–cis* and *cis–trans* photoisomerization processes during exposure to polarized blue-green light.

The phase field photomechanical model predictions also strongly depend on the rate of the liquid crystal domain structure evolution and photoplastic interactions with the polymer network. Stable defect structures are well known to form in liquid and polymeric liquid crystal materials; see ref.[29] for many theoretical examples. However, these stable defect structures depend on certain director constraints on the boundary of a domain. In the liquid crystal polymer phase field model, the “micro” traction is set to zero on all boundaries with no constraint on the director (e.g., rubbed glass interface in a fluidic system). This boundary condition promotes a transition from a polydomain to a monodomain over relatively longer time simulations than considered during photomechanical bending deformation (s). The light induced deformation simulations were conducted on shorter time scales to avoid relaxation to a monodomain state. It is also important to point out that the phase field simulations lead to photoplastic interactions with the polymer network. All bending simulations presented here are irreversible where no recovery of bending occurs since there is no preferred liquid crystal orientation. Photoelastic effects could be considered within the model by including a residual deformation state at the point of polymer cross-linking as described in ref.[45] Experiments have shown that the initial domain structure at cross-linking can strongly influence the soft elastic liquid crystal elastomer response in weakly crosslinked polymer networks.[46]

6. Conclusion

A modeling framework has been presented that couples liquid crystal domain structure evolution, mechanics of glassy polymer networks, and light absorption to quantify differences in bending deformation when assuming *trans–cis* versus an idealized *trans–cis–trans* photoisomerization (i.e., *trans* reorientation). The results illustrate subtle differences in bending deformation that depend on the underlying liquid crystal domain structure reorientation and competing liquid crystal and polymer mechanical energy penalties during bending. Qualitative estimates suggest symmetric bi-directional bending occurs in glassy photomechanical

azobenzene polymer networks that are exposed to blue-green polarized light. The results are important in understanding how to control such materials for larger degree of freedom bending and twisting. In contrast to bending during UV stimulated *trans–cis* and reverse visible light stimulated *cis–trans* processes, polarized blue-green light may provide new avenues for control of morphing structures from a single wavelength of polarized light.

Acknowledgements

The authors gratefully acknowledge support through the DARPA YFA grant N66001-09-1-2105, a sub-contract through the Materials and Manufacturing Directorate of the Air Force Research Laboratory (FA8650-09-D-5434), and an NSF CAREER award (grant number 028796). Any opinions, findings, and conclusions or recommendations expressed in this publication are those of the authors and do not necessarily reflect the views of the funding sponsors.

Supporting Information

Detailed facts of importance to specialist readers are published as ”Supporting Information”. Such documents are peer-reviewed, but not copy-edited or typeset. They are made available as submitted by the authors.

Filename	Description
mats_201100089_sm_supplfigs.pdf 1.7 MB	supplfigs

Please note: The publisher is not responsible for the content or functionality of any supporting information supplied by the authors. Any queries (other than missing content) should be directed to the corresponding author for the article.

References

1 M. Warner, E. Terentjev, *Liquid Crystal Elastomers–Revised Edition*, Oxford Science Publications, Oxford 2007.
Google Scholar

2 Y. Zhao, T. Ikeda, *Smart Light-Responsive Materials*, John Wiley and Sons, Inc., Hoboken 2009.
Wiley Online Library | Web of Science® | Google Scholar

3 T. Ikeda, J. Mamiya, Y. Yu, *Angew. Chem.* 2007, **46**, 506.

Wiley Online Library | CAS | PubMed | Web of Science® | Google Scholar

4 H. Finkelmann, S. Kim, A. Muñoz, P. Palffy-Muhoray, *Adv. Mater.* 2001, **13**, 1069.
Wiley Online Library | CAS | Web of Science® | Google Scholar

5 P. Palffy-Muhoray, W. Cao, M. Moreira, B. Taheri, A. Munoz, *Philos. Trans. R. Soc. A* 2006, **364**, 2747.
Crossref | CAS | PubMed | Web of Science® | Google Scholar

6 J. Harden, B. Mbanga, N. Éber, K. Fodor-Csorba, S. Sprunt, J. Gleeson, A. Jákli, Liquid Crystal Communications, pp. 1– 11, 2006. Online Available: http://www.e-lc.org/docs/2006_07_18_08_47_15 .
Google Scholar

7 I. Rousseau, P. Mather, *J. Am. Chem. Soc.* 2003, **125**, 15300.
Crossref | CAS | PubMed | Web of Science® | Google Scholar

8 W. Lehmann, H. Skupin, C. Tolksdorf, E. Gebhard, R. Zentel, P. Krüger, M. Lösche, F. Kremer, *Nature* 2001, **410**, 447.
Crossref | CAS | PubMed | Web of Science® | Google Scholar

9 C. Spillman, B. Ratna, J. Naciri, *Appl. Phys. Lett.* 2007, **90**, 021911– 1.
Crossref | CAS | Web of Science® | Google Scholar

10 K. Harris, C. Bastiaansen, J. Lub, D. Broer, *Nano Lett.* 2005, **5**, 1857.
Crossref | CAS | PubMed | Web of Science® | Google Scholar

11 R. Lovrien, *Proc. Natl. Acad. Sci.* 1967, **57**, 236.
Crossref | CAS | PubMed | Web of Science® | Google Scholar

12 K. Harris, R. Cuypers, P. Scheibe, C. van Oosten, C. Bastiaansen, J. Lub, D. Broer, *J. Mater. Chem.* 2005, **15**, 5043.
Crossref | CAS | Web of Science® | Google Scholar

13 H. Koerner, T. White, N. Tabiryan, T. Bunning, R. Vaia, *Mater. Today* 2008, **11**, 34.
Crossref | CAS | Web of Science® | Google Scholar

14 M. Dunn, *J. Appl. Phys.* 2007, **102**, 013506– 1.
Crossref | CAS | Web of Science® | Google Scholar

15 K. Long, T. Scott, H. Qi, C. Bowman, M. Dunn, *J. Mech. Phys. Solids* 2009, **57**, 1103.
Crossref | CAS | Web of Science® | Google Scholar

16 M. Warner, L. Mahadevan, *Phys. Rev. Lett.* 2004, **92**, 134302– 1.
Crossref | CAS | PubMed | Web of Science® | Google Scholar

17 C. van Oosten, C. Bastiaansen, D. Broer, *Nat. Mater.* 2009, **8**, 677.
Crossref | CAS | PubMed | Web of Science® | Google Scholar

18 T. Ikeda, J. Mamiya, Y. Yu, *Science* 1995, **268**, 1873.
Crossref | CAS | PubMed | Web of Science® | Google Scholar

19 M. Warner, E. Terentjev, *Macromol. Symp.* 2003, **200**, 81.
Wiley Online Library | CAS | Web of Science® | Google Scholar

20 N. Viswanathan, D. Kim, S. Bian, J. Williams, W. Liu, L. Li, L. Samuelson, J. Kumar, S. Tripathy, *J. Mater. Chem.* 1999, **9**, 1941.
Crossref | CAS | Web of Science® | Google Scholar

21 K.-M. Lee, H. Koerner, R. Vaia, T. Bunning, T. White, *Macromolecules* 2010, **43**, 8185.
Crossref | CAS | Web of Science® | Google Scholar

22 V. Toshchevikov, M. Saphiannikova, G. Heinrich, *J. Phys. Chem. B* 2009, **113**, 5032.
Crossref | CAS | PubMed | Web of Science® | Google Scholar

23 D. Corbett, M. Warner, *Phys. Rev. Lett.* 2006, **96**, 237802.
Crossref | PubMed | Web of Science® | Google Scholar

24 C. van Oosten, K. Harris, C. Bastiaansen, D. Broer, *Eur. Phys. J. E* 2007, **23**, 329.
Crossref | CAS | PubMed | Web of Science® | Google Scholar

25 D. Statman, I. Janossy, *J. Chem. Phys.* 2003, **118**, 3222.
Crossref | CAS | Web of Science® | Google Scholar

26 D. Corbett, M. Warner, *Phys. Rev. E* 2008, **77**, 051710.
Crossref | PubMed | Web of Science® | Google Scholar

27 D. Anderson, D. Carlson, E. Fried, *J. Elast.* 1999, **56**, 3356.
Crossref | Web of Science® | Google Scholar

28 W. Oates, H. Wang, *Model. Simul. Mater. Sci. Eng.* 2009, **17**, 064004.
Crossref | CAS | Web of Science® | Google Scholar

29 P. de Gennes, J. Prost, *The Physics of Liquid Crystals*, Oxford Science Publications, Oxford 1993.
Google Scholar

30 J. Ericksen, *Arch. Ration. Mech. Anal.* 1991, **113**, 97.
Crossref | Web of Science® | Google Scholar

31 E. Virga, *Variational Theories for Liquid Crystals*, Chapman & Hall, London 1994.
Crossref | Google Scholar

32 E. Fried, S. Sellers, *J. Chem. Phys.* 2006, **124**, 024908.
Crossref | CAS | PubMed | Web of Science® | Google Scholar

33 S. Conti, A. DeSimone, G. Dolzmann, *J. Mech. Phys. Solids* 2002, **50**, 1431.
Crossref | CAS | Web of Science® | Google Scholar

34 A. DeSimone, L. Teresi, *Eur. Phys. J. E* 2009, **29**, 191.
Crossref | CAS | PubMed | Web of Science® | Google Scholar

35 C. Eisenbach, *Makromol. Chem.* 1978, **179**, 2489.
Wiley Online Library | CAS | Web of Science® | Google Scholar

36 T. Fujino, T. Tahara, *J. Phys. Chem. A* 2000, **104**, 4203.
Crossref | CAS | Web of Science® | Google Scholar

37 T. White, S. Serak, N. Tabiryan, R. Vaia, T. Bunning, *J. Mater. Chem.* 2009, **19**, 1045.
Crossref | Google Scholar

38 S. Serak, N. Tabiryan, R. Vergara, T. White, J. White, R. Vaia, T. Bunning, *Soft Matter* 2010, **6**, 779.
Crossref | CAS | Web of Science® | Google Scholar

39 L. Malvern, *Introduction to the Mechanics of a Continuous Medium*, Prentice-Hall, Inc., Englewood Cliffs, NJ 1969.
Google Scholar

40 A. Eringen, G. Maugin, *Electrodynamics of Continua I: Foundations and Solid Media*, Springer-Verlag, New York 1990.
Crossref | Google Scholar

41 M. Irie, Y. Hirano, S. Hashimoto, K. Hayashi, *Macromolecules* 1981, **14**, 262.
Crossref | CAS | Web of Science® | Google Scholar

42 G. R. Fowles, Introduction to Modern Optics, Dover, 1989.
Google Scholar

43 R. Loudon, *The Quantum Theory of Light*, Clarendon Press, Oxford 1973.
Google Scholar

44 G. Holzapfel, *Nonlinear Solid Mechanics*, Wiley & Sons, Inc., Chichester 2000.
Google Scholar

45 J. Biggins, M. Warner, K. Bhattacharya, *Phys. Rev. Lett.* 2009, **103**, 037802– 1.
Crossref | CAS | PubMed | Web of Science® | Google Scholar

46 K. Urayama, E. Kohmon, M. Kojima, T. Takigawa, *Macromolecules* 2009, **42**, 4084.
Crossref | CAS | Web of Science® | Google Scholar

Citing Literature

Download PDF